[Materials Today: Proceedings]

Classical laminate theory for flexural strength prediction of FDM 3D printed PLAs

Shilpesh R. Rajpurohit[a1], Harshit K. Dave[b], Mahdi Bodaghi[c]

[a]*Department of Mechanical Engineering, B K Birla Institute of Engineering and Technology, Pilani – 333031, India*
[b]*Department of Mechanical Engineering, Sardar Vallabhbhai National Institute of Engineering and Technology, Surat – 395007, India*
[c]*Department of Engineering, School of Science and Technology, Nottingham Trent University, Nottingham - NG11 8NS, UK*

Abstract

Fused Deposition Modeling (FDM) is a prominent Additive Manufacturing (AM) technology for producing tailored components with complicated geometries, particularly from thermoplastics. Due to poor mechanical performance and printed component quality, this technology was limited in its capacity to make parts for industrial applications. As a result, researchers are being encouraged to improve the mechanical performance of FDM components in order to meet the huge demand for functional components. The selection of process variables has a considerable effect on the mechanical performance of FDM products. Therefore, the correlation between the mechanical properties and process variables should be evaluated. This paper highlights the flexural strength of the FDM parts at different raster orientation and describe the flexural strength through classical laminate theory (CLT). The elastic constant was derived for unidirectional (UD) UD0°, UD45°, and UD90° plies at various layer height and raster width combinations. The constitutive models were developed using experimentally derived elastic constant to calculate the flexural strength of the UD0°, UD45°, and UD90° parts and the results were validated against the experimental value. Furthermore, flexural strength was analyzed at various raster orientation for different combinations of layer height and raster width. Results show that experimentally measured flexural strength decreases with raster orientation and can be estimated by CLT model. The nature of failure under flexural loads was further investigated using fractography analysis of failure surfaces for FDM laminates.

Keywords: Fused deposition modeling, Classical laminate theory, flexural strength, raster orientation, layer height, raster width

1. Introduction

3D Printing (3DP) enables the layer-by-layer creation of complicated components directly from digital data without the need of any tool. 3D printing technology is widely accepted in the many fields of engineering and technology owing to its advantages of faster production and better production cost over to traditional way of manufacturing [1]. Fused Deposition Modeling (FDM) is a prominent 3DP technology, used to produce functional complex polymer geometries. Wherein, the polymer filament is melted into semi solid stated in a liquefier head and afterwards strategically dispensed through a nozzle on bed or previously deposited layer. The FDM nozzle follows the cross-sectional geometry of the component to generate 3D parts directly from a CAD model [2,3].

FDM produced parts are frequently utilized in variety of sectors, such as engineering, manufacturing, industrial, automobile, aerospace, healthcare and construction industries. However, the use of FDM parts is constrained due to the poor mechanical properties, anisotropic mechanical properties, weak layer bonding, voids in the printed parts as compared to injection moulding processed parts [4]. The mechanical performance of FDM components is determined by the FDM process parameters used. Therefore, a reasonable selection of process parameters that impact the mechanical characteristics of FDM components and improve the qualitative and quantitative qualities of printed parts is required [5,6].

Over the last several years, several researchers have attempted to investigate the influence of the FDM variables on the enhancement of mechanical properties of FDMed parts. Further, the attempt has also been made to predict the mechanical properties of FDM parts by different researchers. The impact of process factors on the tensile characteristics of FDM-produced PP and glass fibre reinforced PP was examined by Carneiro et al. [7]. They reported that the degree of infill and filament orientation have a substantial impact on the tensile strength. Vicente et al. [8] examined the effect of FDM parameters on the tensile properties of ABS components. The increment in nozzle diameter, infill density leads to increment in tensile properties. Further, lower value of layer height and ± 45°/45° raster angle promotes the higher value of tensile strength and stiffness. Sood et al. [9] evaluated the mechanical properties of FDM produced part. Larger layer height, smaller raster angle, thick raster and zero air gap help to achieve the higher tensile, flexural and impact strength. Zhang et al. [10] developed a data driven

[1]*E-mail address: shilpeshrajpurohit@gmail.com*

predictive model using deep learning structure for tensile strength prediction. The Long Short-term Memory (LSTM) network has shown better prediction capability compared to Random Forest (RF) and Support Vector Regression (SVR) models. An anisotropy in the tensile characteristics of FDM produced ABS was investigated by Ahn et al. [11]. Xu et al. [12] explored the influence of the process parameters on flexural properties of FDM produced Polyetherketoneketone (PEKK) parts. They reported that with decrement in layer height and increment in infill percentage, flexural properties are improved.

Rajpurohit et al. [13] predicted and experimentally validated the tensile properties of the 3D printed PLA through CLT for distinct raster angle. They obtained a good agreement between the tensile strength measured through CLT and experiments. They also reported that higher tensile strength observed for 0° raster angle. Malagutti et al. [14] applied the CLT to anticipate the tensile properties of FDM processed wood flour filled polyester composites. They also reported the good agreement in measured properties with theoretical predictions. Somireddy et al. [15] concluded that CLT could be utilized to describe the mechanical properties of the FDM parts. Nasirov et al. [16] applied the asymptotic homogenization and CLT for estimation of mechanical properties of FDM made parts. Gokulakrishnan and Saravana Kumar [17] developed a computation model using CLT and corelated with experiments to describe the flexural properties. Somireddy et al. [18] did experimental and analytical study to assess the flexural behavior of the FDM parts. They confirmed that CLT could be utilized to describe the mechanical properties of the printed laminates. Mishra and P [19] evaluate the in-plane stiffness of FDM bi-material laminates at different raster angle through CLT. They found that bi-material laminate printed with 0° raster angle displayed the higher in-plane stiffness and ultimate tensile strength. Casavola et al. [20] described the mechanical properties of FDM produced parts as a function stacking sequence through CLT. They reported that Young's modulus is reduced as raster angle is increasing from 0° to 90°. Further, CLT model has high capacity of prediction and experimental results and CLT results have close agreement with an error in the range of 4.7% to 6.6%. Alaimo et al. [21] described the mechanical properties of FDM produced part though CLT. Saeed et al. [22] predicted the tensile properties of carbon fiber reinforced FDM printed nylon composite using CLT approach.

According to the literature review, the mechanical characteristics of FDM produced components are greatly influenced by the process parameters and meso-structure of the printed parts. Furthermore, it is discovered that CLT may be utilized efficiently to forecast the mechanical characteristics of FDM printed objects. The majority of current research has focused on the effect of process parameters on tensile characteristics and the capacity of CLT to forecast the tensile qualities of FDM laminates. There has been little research on the flexural characteristics of FDM components and the use of CLT in predicting flexural properties. In this study, an experimental and analytical research of the flexural characteristics of FDM printed PLA is conducted. Effect of the process variables (e.g., layer height, raster width and raster angle) on the flexural strength of FDM printed PLA has been assessed. Further, the CLT model was derived to anticipate the flexural properties of the FDM laminates and has been corroborated through experimental results. Additionally, fractography analysis of failure surface for FDM laminates has also been done to investigate the failure mechanism under flexural loading.

2. Classical Laminate Theory

CLT is a descriptive method for analyzing the coupling effect in composite laminates. CLT can anticipate stresses, displacements, and curvatures induced inside the laminate as a consequence of mechanical loads [23,24]. A lamina's constitutive relation is as follows:

$$\begin{Bmatrix}\sigma_{11}\\ \sigma_{22}\\ \tau_{12}\end{Bmatrix}=\begin{bmatrix}Q_{11} & Q_{12} & 0\\ Q_{12} & Q_{22} & 0\\ 0 & 0 & Q_{66}\end{bmatrix}\begin{Bmatrix}\varepsilon_{11}\\ \varepsilon_{22}\\ \gamma_{12}\end{Bmatrix} \quad (1)$$

The terms in the matrix are

$$Q_{11}=\frac{E_1}{1-\upsilon_{12}\upsilon_{21}}, Q_{12}=\frac{\upsilon_{21}E_1}{1-\upsilon_{12}\upsilon_{21}}, Q_{22}=\frac{E_2}{1-\upsilon_{12}\upsilon_{21}}$$

$$Q_{66}=G_{12} \text{ with}$$

$$\upsilon_{21}=\upsilon_{12}\frac{E_2}{E_1}$$

Where, E_1 and E_2 are the elastic modulus, υ_{12} and υ_{21} are Poisson's ratio, G_{12} is shear modulus.

The resulting force and moment per unit width in the laminate with N numbers of layer is stated as follows:

$$\begin{Bmatrix}N_{xx}\\ N_{yy}\\ N_{xy}\end{Bmatrix}=\int_{-h/2}^{h/2}\begin{Bmatrix}\sigma_{xx}\\ \sigma_{yy}\\ \sigma_{xy}\end{Bmatrix}dz=\sum_{K=1}^{N}\int_{h_k}^{h_{k+1}}\begin{Bmatrix}\sigma_{xx}\\ \sigma_{yy}\\ \tau_{xy}\end{Bmatrix}dz, \{N\}=\sum_{K=1}^{N}\int_{h_k}^{h_{k+1}}\{\sigma\}dz \quad (2)$$

$$\begin{Bmatrix} M_{xx} \\ M_{yy} \\ M_{xy} \end{Bmatrix} = \int_{-h/2}^{h/2} \begin{Bmatrix} \sigma_{xx} \\ \sigma_{yy} \\ \sigma_{xy} \end{Bmatrix} dz = \sum_{K=1}^{N} \int_{h_k}^{h_{k+1}} \begin{Bmatrix} \sigma_{xx} \\ \sigma_{yy} \\ \tau_{xy} \end{Bmatrix} dz, \{M\} = \sum_{K=1}^{N} \int_{h_k}^{h_{k+1}} \{\sigma\} z dz \quad (3)$$

Where, N_{xx} and N_{yy} is the normal force per unit width in the x and y direction, N_{xy} is a shear force, M_{xx} and M_{yy} is the bending moment yz and xz planes, M_{xy} is the twisting moment

Using equation (1), equations (2) and (3) become

$$\{N\} = \sum_{K=1}^{N} [\bar{Q}] \left[\int_{h_k}^{h_{k+1}} \{\varepsilon^0\} dz + \int_{h_k}^{h_{k+1}} \{k\} z dz \right] \quad (4)$$

$$\{N\} = [A]\{\varepsilon^0\} + [B]\{k\} \quad (5)$$

$$\{M\} = \sum_{K=1}^{N} [\bar{Q}] \left[\int_{h_k}^{h_{k+1}} \{\varepsilon^0\} z\, dz + \int_{h_k}^{h_{k+1}} \{k\} z^2 dz \right] \quad (6)$$

$$\{M\} = [B]\{\varepsilon^0\} + [D]\{k\} \quad (7)$$

Where, In-plane stiffness is denoted by matrix [A], bending stiffness coupling is denoted by matrix [B], and bending stiffness is denoted by matrix [D].

The matrices [A], [B], and [D] are stated as follows:

$$[A] = \sum_{k=1}^{N} [\bar{Q}] \int_{h_k}^{h_{k+1}} dz \quad (8)$$

$$[B] = \sum_{k=1}^{N} [\bar{Q}] \int_{h_k}^{h_{k+1}} z dz \quad (9)$$

$$[D] = \sum_{k=1}^{N} [\bar{Q}] \int_{h_k}^{h_{k+1}} z^2 dz \quad (10)$$

Due to the coupling matrix [B] = 0, there is no extension bending coupling in the case of symmetric laminate. Then, from equation (7), the strains for a symmetric laminate are as follows:

$$\begin{Bmatrix} k_{xx} \\ k_{yy} \\ k_{xy} \end{Bmatrix} = [D]^{-1} \begin{Bmatrix} M_{xx} \\ M_{yy} \\ M_{xy} \end{Bmatrix} \quad (11)$$

When, flexural stress is applied in z-direction for laminate thickness h, then the in-plane bending moment for this load situation becomes $M_{xx} \neq 0$ M_{yy}= 0 and M_{xy}= 0. The stress-strain relation for the flexural test is ${\sigma^f}_{xx} = {E^f}_{xx}\varepsilon^f_{xx}$, using these relationships the modulus of elasticity in the x-direction is calculated using these equations

$${E^f}_{xx} = \frac{12}{[D^{-1}]_{11} h^3} \quad (12)$$

To determine E_{xx} of the laminate, it is necessary to have the lamina's elastic modulus such as E_1, E_2, G_{12} and υ_{12}. The laminate consecutive equation is expressed as follows:

$$\begin{Bmatrix} N \\ M \end{Bmatrix} = \begin{bmatrix} A & B \\ B & D \end{bmatrix} \begin{Bmatrix} \varepsilon^0 \\ \kappa \end{Bmatrix} \quad (13)$$

For a test specimen in bending sole non-zero elements of N and M is M_{xx}. As a result, equation (13) is reduced to

$$\begin{Bmatrix} 0 \\ M \end{Bmatrix} = \begin{bmatrix} A & B \\ B & D \end{bmatrix} \begin{Bmatrix} \varepsilon^0 \\ \kappa \end{Bmatrix} \quad (14)$$

in which,

$$M = \begin{bmatrix} M_{xx} \\ 0 \\ 0 \end{bmatrix} \quad (15)$$

3. Experimental Methodology

Four elastic constants are needed, as was previously mentioned, to evaluate an orthotropic lamina bearing plane

tensions. These characteristics can be determined by performing tensile test on specimens with raster angles of UD0°, UD90°, and UD45° at various layer height and raster width configurations, as shown in the Table 1 and Table 2. The test samples were created from PLA material on an open-source FDM based 3D printer.

With a longitudinal sample at UD0°, the longitudinal elastic modulus E_1 and poison ratio υ_{12} are calculated, while the transverse elastic modulus E_2 is calculated with a transverse specimen at UD90°. Elastic modulus E_{45}, which is utilized to compute the shear modulus of G_{12} is determined from a specimen with raster orientation θ = UD45°.

$$G_{12} = \left[\frac{4}{E_{45}} - \frac{1}{E_1} - \frac{1}{E_2} + \frac{2\upsilon_{12}}{E_1}\right]^{-1} \tag{16}$$

Equation (16) was utilized together with other experimentally acquired elastic constants E_1, E_2 and υ_{12} to obtain the in-plane shear modulus G_{12}.

These elastic constants have been utilized to develop CLT model which is used to estimate the flexural performance of the FDM parts. These elastic constants were derived by applying uniaxial tensile loading at UD0°, UD45°, and UD90° plies at different combination of layer height and raster width. To examine the impact of the filament cross-section, nine various configurations of layer height and raster width were taken into consideration and evaluated, as indicated in Table 1. The tensile test samples have been printed and tested in accordance with ASTM D638 standard. PLA samples were evaluated using a Tinius Olsen H50KL UTM with computer control and data capture. The test speed was adjusted to 5 mm/min as per ASTM D638 standard and tested until it failed.

Table 1 Process parameters and their levels

Parameters	Levels		
	1	2	3
Raster angle (°)	0	45	90
Layer height (mm)	0.1	0.2	0.3
Raster width (mm)	0.5	0.6	0.7

Table 2 Constant process parameters

Parameters	Levels
Print temperature (°C)	210
Bed temperature (°C)	70
Print speed (mm/s)	50
No. of perimeter	1
Degree of infill (%)	100
Nozzle diameter (mm)	0.4
Infill pattern	Unidirectional rectilinear

The goal of this study is to explore the flexural behaviour of the FDM processed PLA subjected to different print parameters such as raster angle, layer height and raster width on flexural strength through experimental study and CLT model. To compare the experimental and CLT results of flexural performance, specimens with 0°, 45°, and 90° raster orientations were manufactured and evaluated for various combinations of layer height and raster width. Table 1 and Table 2 displays the specified process variables and their levels, as well as the fixed process parameters that are taken into consideration during the printing of flexural specimens. In this study, three parameters have been modified at three levels. Therefore, in accordance with the full factorial experimental design, 27 trials need to be undertaken with diverse experiment conditions. All experiments were repeated twice to ensure the accuracy and repeatability. According to ASTM D790, the three-point bend test was carried out on a Tinus Olsen H50KL UTM. The samples used in this investigation are a rectangular block with the following measurements: 127 mm x 12.7 mm x 3.2 mm. The schematic representation and actual three-point bending test is shown in Figure 1.

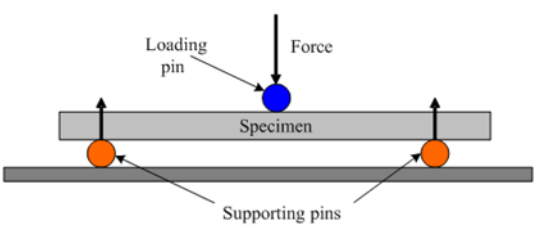

(a)

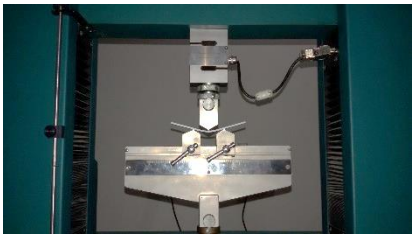

(b)

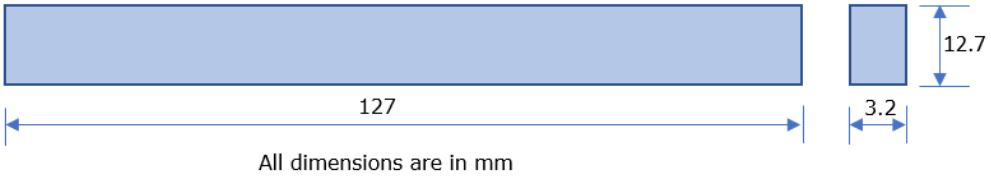

(c)

Figure 1 Flexural testing set up and flexural specimen

4. Results and Discussions

All of the tests were carried out in accordance with the previously described full factor experimental design. Figure 2 display the mean effect plot of process variables on the flexural strength of PLA specimens. It is demonstrated that as the raster angle and layer height increases, flexural strength decreases. It was observed that the flexural strength is higher at 0° raster angle and got reduced as the raster angle increased. The specimens with a raster angle of 0° exhibits greater interlayer bonding than specimens with other angles, and the printed layers are parallel to the bending plane, increasing the specimen's resistance to bending. Due to the stronger adhesion between layers, a higher flexural strength can be observed at a lower layer height. A substantially stronger bond results from more layer-to-layer bonding at lower layer heights. A semi-solid raster needs a higher extrusion pressure at a lower layer height for proper deposition. The contact between the two layers is ensured by the higher pressure produced as a result of the lower layer height, ultimately leading to a stronger adhesion.

On the contrary, subject to raster width, flexural strength is increased with raster angle up to 0.6 mm and then after it start decreasing. The flexural strength is increases with an increase in raster width up to 0.6 mm until it starts decreasing. Because of the greater thermal mass, the raster cools more slowly and remains above the glass transition temperature for a longer period of time. As a result, the bond between the adjacent raster, is strengthened, increasing the bond strength. The adhesion strength is strengthened because the raster with wider width has higher surface area in contact with layers.

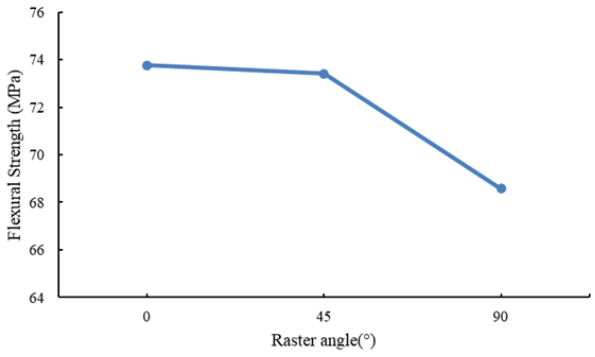

(a)

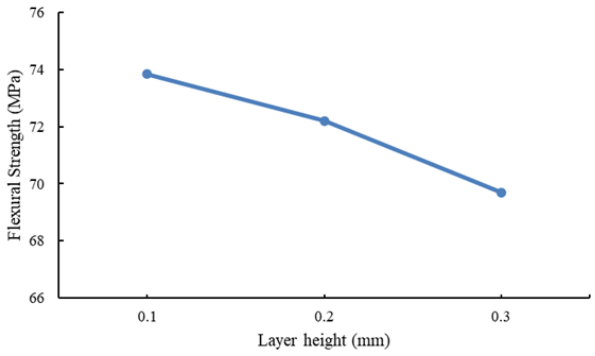

(b)

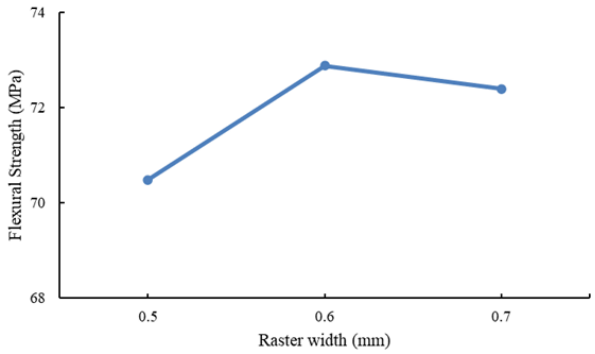

(c)

Figure 2 Mean effect of process variables on flexural strength (a) raster angle, (b) layer height and (c) raster width

The microscopic investigation of the failure surface was employed to evaluate the failure mechanism under flexural loading. The microscopic views of the damaged surfaces are displayed in Figure 3 to Figure 5. Figure 3(a) depicts the fractured structure for a sample with a 0° raster angle. It demonstrates that failure begins on the tensile side but that on the compression side, intact rasters keep the elements of the failure together. The specimen constructed with a 0° raster angle exhibits nearly linear fracture propagation along the applied load. Additionally, the raster printed at the appropriate inclination angle resulted in a raster of a reduced length under bending stress, and its bending resistance decreased as the raster angle changed to 45° and 90°. Figure 3(b) and Figure 3(c), respectively, display the failure morphologies for samples with 45° and 90° raster angles. The specimen with 90° raster orientations exhibits the minimal amount of bending resistance. The bonding between the rasters, which is relatively weaker than a monofilament, is what allows cracks to spread along the raster deposition. Figure 4(a) depicts failure morphologies for a specimen with a 0.1 mm layer height. It demonstrates that failure proceeds on the tensile side, but that the pieces are kept together by intact compression side rasters. It is demonstrated that a wide stress whitening provides higher resistance to the bending strain. Small raster stretching caused a catastrophically brittle failure for the 0.2 mm and 0.3 mm layer heights, suggesting poor resilience to bending. For a specimen with a 0.5 mm raster width, catastrophic and brittle failure can be seen in Figure 5 (a). The intact layers on the compression side kept the parts together, but the fracture started from the bottom layers, which were subjected to tensile stress. Wide stress whitening (Figure 5(b)) is demonstrated for the 0.6 mm raster width, which provides greater bending resistance.

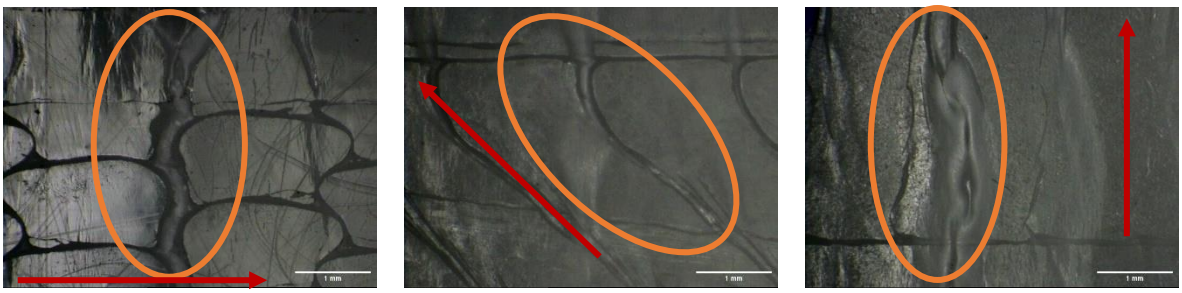

(a) (b) (c)

Figure 3 Close view of the fractured surface of specimens after flexural testing at raster angle of (a) 0°, (b) 45° and (c) 90°

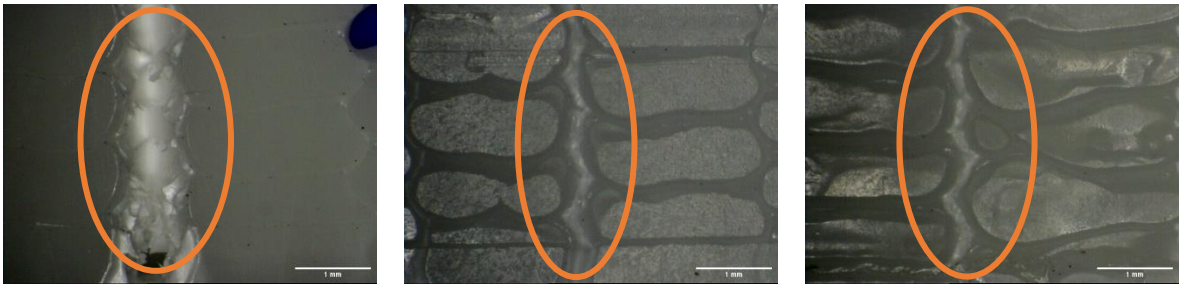

(a) (b) (c)

Figure 4 Close view of the fractured surface of specimens after flexural testing at layer height of (a) 0.1 mm, (b) 0.2 mm and (c) 0.3 mm

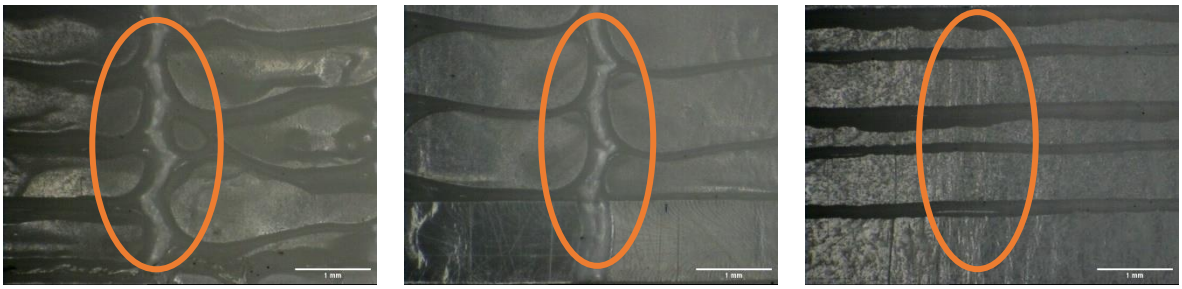

(a) (b) (c)

Figure 5 Close view of the fractured surface of specimens after flexural testing at raster width of (a) 0.5 mm, (b) 0.6 mm and (c) 0.7 mm

The modulus of elasticity was calculated using the uniaxial tensile test results. Table 3 shows the elastic characteristics found experimentally for various setups of layer height and raster width. It can be seen that elastic constants are dependent on the printing parameters. Elastic constants are in general found to be increased with increment in raster angle and layer height. On the other hand, it is increased with increment in raster width and then deceasing. At the different combination of the layer height and raster width, the elastic constants are significantly affected and displayed incomprehensible behaviour may be due to the presence of voids, reduced cross section area or ineffective inter-filament bonding. These elastic constants are used to develop a CLT model which is predicting the flexural performance of the FDM produced PLA specimens. Flexural specimens were printed at 0°, 45° and 90° raster angle with various configuration of layer height and raster width. Furthermore, flexural testing was performed to calculate the flexural strength of the samples. Then after the experimental flexural strengths were tested with the flexural strength calculated using CLT to verify the CLT model. The experimental and calculated flexural strengths are shown versus the raster angle as displayed in Figure 6 for various configuration of raster width and layer height. Overall, it can be observed that experimental findings and CLT calculations are in good accord. However, the experimental and CLT results, deviate further when the layer height and raster width are greater values. In numerous test scenarios, the flexural strength decreases when the raster angle is increased. As can be observed, 0° raster angle yields the highest flexural strength, compared to 45° and 90° raster angles. An increment in layer height and raster width leads to reduction in the flexural strength. It may be due to the higher value of layer height and raster width, a large proportion of voids and a considerable decrement in bonding area that may cause a decrease in strength. The CLT might be utilized to describe the flexural strength of the FDM components as it can be seen from Figure 6 that the results are corresponding to those of experimental results.

Table 3 Elastic constant for CLT model

Layer height (mm)	0.1			0.2			0.3		
Raster width (mm)	0.5	0.6	0.7	0.5	0.6	0.7	0.5	0.6	0.7
$E_1\ (MPa)$	757	886	749	761	779	737	828	717	895
$E_2\ (MPa)$	721	828	751	532	737	844	773	643	638
$G_{12}(MPa)$	334	335	294	305	205	238	272	244	177
ν_{12}	0.34	0.34	0.34	0.34	0.34	0.34	0.34	0.34	0.34

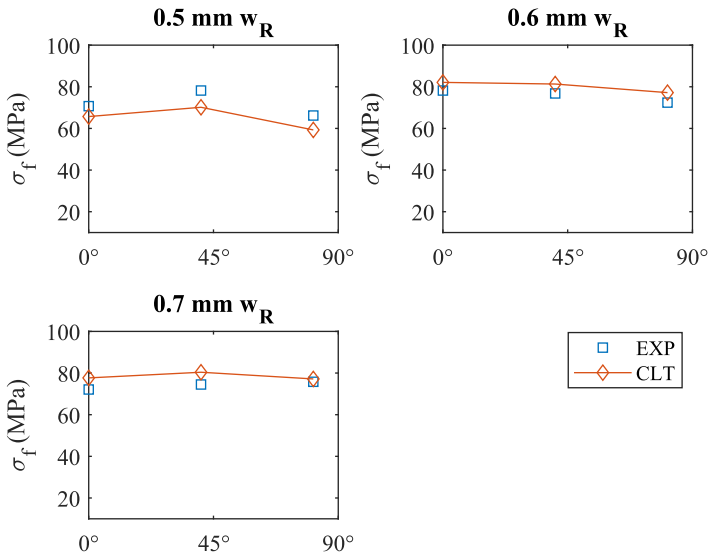
0.5 mm w_R
0.6 mm w_R
0.7 mm w_R
σ_f (MPa)
100
80
60
40
20
0°
45°
90°
EXP
CLT

(a)

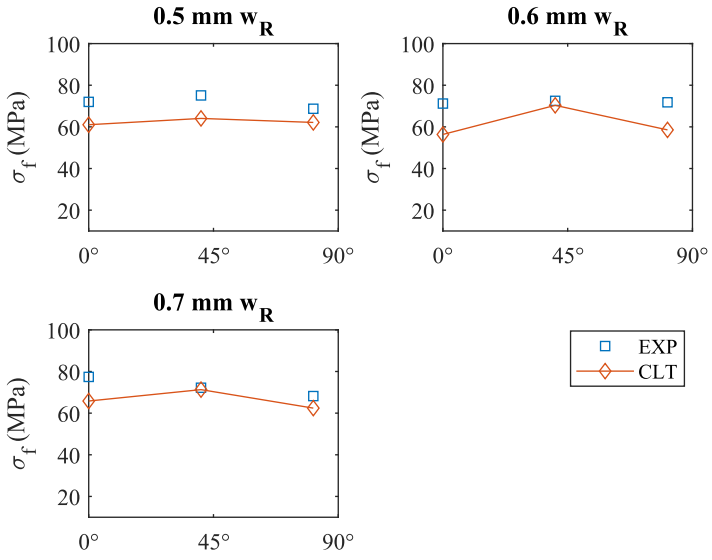
0.5 mm w_R
0.6 mm w_R
0.7 mm w_R
σ_f (MPa)
100
80
60
40
20
0°
45°
90°
EXP
CLT

(b)

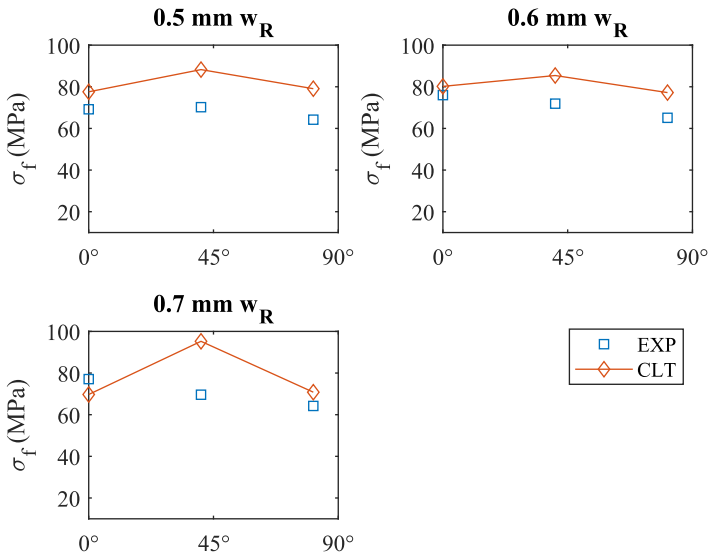

(c)

Figure 6 Comparison between CLT derived and experimental flexural strength at layer height of (a) 0.1 mm, (b) 0.2 mm and (c) 0.3 mm

5. Conclusions

In this research work, performance of the FDM printed PLA has been investigated subjected to flexural loading. Further, the application of the CLT model has also been investigated to illustrate the efficacy of the CLT model in predicting the flexural properties of the printed specimens. Based on the experimental study, it is possible to deduce that flexural strength is significantly influenced by the section of the process parameters. Flexural strength is reduced as raster angle and layer height is increase. At 0° raster angle, failure was predominantly caused due to the stretching and rupture of the deposited beads. However, at 90° raster angle, failure take place parallel to raster deposition through shear bonding between adjacent raster. A higher extrusion pressure was employed during the deposition of layer with lower layer height resulted into improved layer bonding which enhance the flexural strength. Because of the higher thermal mass that cools slowly at the intermediate value of the raster width, a higher flexural strength was obtained and improving the bonding between the raster. Furthermore, the flexural strength of the FDM printed PLA specimens was predicted using CLT, and the results acquired by CLT calculation confirmed validated using experimental results. The experimental flexural finding is consistent with the CLT calculations. As a result, the CLT can be used to estimate the flexural properties of FDM produced components.

References

[1] Mohamed OA, Masood SH, Bhowmik JL. Optimization of fused deposition modeling process parameters: a review of current research and future prospects. *Advances in Manufacturing*, 2015;3(1):42-53. https://doi.org/10.1007/s40436-014-0097-7

[2] Rajpurohit SR, Dave HK. Analysis of tensile strength of a fused filament fabricated PLA part using an open-source 3D printer. *The International Journal of Advanced Manufacturing Technology*. 2019;101(5):1525-36. https://doi.org/10.1007/s00170-018-3047-x

[3] Rajpurohit SR, Dave HK. Impact strength of 3D printed PLA using open source FFF-based 3D printer. *Progress in Additive Manufacturing*. 2021;6(1):119-31. https://doi.org/10.1007/s40964-020-00150-6

[4] Hsueh MH, Lai CJ, Wang SH, Zeng YS, Hsieh CH, Pan CY, Huang WC. Effect of printing parameters on the thermal and mechanical properties of 3d-printed PLA and PETG, using fused deposition modeling. *Polymers*. 2021;13(11):1758. https://doi.org/10.3390/polym13111758

[5] Hsueh MH, Lai CJ, Chung CF, Wang SH, Huang WC, Pan CY, Zeng YS, Hsieh CH. Effect of Printing Parameters on the Tensile Properties of 3D-Printed Polylactic Acid (PLA) Based on Fused Deposition Modeling. *Polymers*. 2021;13(14):2387. https://doi.org/10.3390/polym13142387

[6] Ahmad MN, Ishak MR, Mohammad Taha M, Mustapha F, Leman Z, Anak Lukista DD, Ghazali I. Application of Taguchi Method to Optimize the Parameter of Fused Deposition Modeling (FDM) Using Oil Palm Fiber Reinforced Thermoplastic Composites. *Polymers.* 2022;14(11):2140. https://doi.org/10.3390/polym14112140

[7] Carneiro OS, Silva AF, Gomes R. Fused deposition modeling with polypropylene. *Materials & Design*. 2015;

83:768-76. https://doi.org/10.1016/j.matdes.2015.06.053
[8] Vicente CM, Martins TS, Leite M, Ribeiro A, Reis L. Influence of fused deposition modeling parameters on the mechanical properties of ABS parts. *Polymers for Advanced Technologies*. 2020;31(3):501-507. https://doi.org/10.1002/pat.4787
[9] Sood AK, Ohdar RK, Mahapatra SS. Parametric Appraisal of Mechanical Property of Fused Deposition Modelling Processed Parts. *Materials & Design*. 2010;31(1):287-95. https://doi.org/10.1016/j.matdes.2009.06.016
[10] Zhang J, Wang P, Gao RX. Deep Learning-Based Tensile Strength Prediction in Fused Deposition Modeling. *Computers in Industry*. 2019; 107:11-21. https://doi.org/10.1016/j.compind.2019.01.011
[11] Ahn, S., Montero, M., Odell, D., Roundy, S. and Wright, P.K. Anisotropic material properties of fused deposition modeling ABS. *Rapid Prototyping Journal*. 2002;8(4):248-257. https://doi.org/10.1108/13552540210441166
[12] Xu C, Cheng K, Liu Y, Wang R, Jiang X, Dong X, Xu X. Effect of processing parameters on flexural properties of 3D‐printed polyetherketoneketone using fused deposition modeling. *Polymer Engineering & Science*. 2021;61(2):465-476. https://doi.org/10.1002/pen.25590
[13] Rajpurohit SR, Dave HK, Rajurkar KP. Prediction of tensile strength of fused deposition modeling (FDM) printed PLA using classic laminate theory. Engineering Solid Mechanics. 2022;10(1):13-24. http://dx.doi.org/10.5267/j.esm.2021.12.002
[14] Malagutti L, Mazzanti V, Mollica F. Tensile properties of FDM 3D-printed wood flour filled polymers and mathematical modeling through classical lamination theory. Rapid Prototyping Journal. 2022;28(9):1834-1842. https://doi.org/10.1108/RPJ-11-2021-0298
[15] Somireddy M, Czekanski A. Mechanical characterization of additively manufactured parts by FE modeling of mesostructure. *Journal of Manufacturing and Materials Processing*. 2017;1(2):18. https://doi.org/10.3390/jmmp1020018
[16] Nasirov A, Hasanov S, Fidan I. Prediction of Mechanical Properties of Fused Deposition Modeling Made Parts Using Multiscale Modeling and Classical Laminate Theory. *2019 International Solid Freeform Fabrication Symposium.* 2019. http://dx.doi.org/10.26153/tsw/17367
[17] Gokulakrishnan J, Saravana Kumar G. Experimental and Numerical Investigation of the Flexural Behavior of Fused Deposition Modeling Parts. *In: Shunmugam, M., Kanthababu, M. (eds) Advances in Additive Manufacturing and Joining. Lecture Notes on Multidisciplinary Industrial Engineering. Springer, Singapore*. 2020;347-355. https://doi.org/10.1007/978-981-32-9433-2_31
[18] Somireddy M, de Moraes DA, Czekanski A. Flexural Behavior of FDM Parts: Experimental, Analytical and Numerical Study. *2017 International Solid Freeform Fabrication Symposium 2017.*
[19] Mishra PK, Senthil P. Prediction of In-Plane Stiffness of Multi-Material 3D Printed Laminate Parts Fabricated by FDM Process Using CLT and Its Mechanical Behaviour Under Tensile Load. *Materials Today Communications*. 2020; 23:100955. https://doi.org/10.1016/j.mtcomm.2020.100955
[20] Casavola C, Cazzato A, Moramarco V, Pappalettere C. Orthotropic Mechanical Properties of Fused Deposition Modelling Parts Described by Classical Laminate Theory. *Materials & Design*. 2016; 90:453-8. https://doi.org/10.1016/j.matdes.2015.11.009
[21] Alaimo G, Marconi S, Costato L, Auricchio F. Influence of meso-structure and chemical composition on FDM 3D-printed parts. *Composites Part B: Engineering*. 2017; 113:371-80. https://doi.org/10.1016/j.compositesb.2017.01.019
[22] Saeed K, McIlhagger A, Harkin-Jones E, Kelly J, Archer E. Predication of the in-plane mechanical properties of continuous carbon fibre reinforced 3D printed polymer composites using classical laminated-plate theory. *Composite Structures*. 2021; 259:113226. https://doi.org/10.1016/j.compstruct.2020.113226
[23] Jones, R.M., (2014). Mechanics of composite materials. CRC Press.
[24] Kaw, A.K., (2005). Mechanics of composite materials. CRC Press.